scientific reports

Check for updates

OPEN

A virtual simulation study of the effects of laparotomy incision location and wound stiffness on abdominal wall mechanics

Lluís Tuset[1], Manuel López-Cano[2], Gerard Fortuny[1], Josep M. López[1], Joan Herrero[3] & Dolors Puigjaner[1]✉

Incisional hernia (IH) is a common complication of laparotomy surgical procedures, influenced by factors such as incision location and surgical wound (SW) tissue strength, and the intra-abdominal pressure (IAP) levels the patient is subject to. In this study we use finite element simulations to investigate how these factors affect the abdominal wall (AW) deformation and the stress distribution on the tissues. Comprehensive geometric models of the AW were generated for five laparotomy incisions, namely midline, paramedian, pararectus, transverse supraumbilical, and subcostal oblique. Finite element simulations for IAP values between 4 and 20 kPa and with the SW tissue strength ranging from very soft to very stiff were conducted using the code Aster open-source software. Simulations revealed that as a general rule laparotomy incisions significantly impact AW mechanics when the SW tissue is soft. In particular, AW mechanics is more sensitive to SW strength in vertical incisions (midline, paramedian, pararectus). The resulting change of the SW dimensions with increasing IAP was also investigated. Softening the SW tissue led to substantial volume increases of the vertical incisions for a given IAP level. In addition, we analyzed stress levels in the SW tissue as well as in the surrounding muscles. A very soft SW may induce the appearance of regions with very high stress levels in the surrounding muscle tissue, heightening their rupture risk. This effect was especially noticeable for the midline incision. On the overall, we found that when the SW tissue is too tender transverse supraumbilical and subcostal incisions present the lowest risk of tissue ruptures whereas the midline incision is the most vulnerable one and the paramedian and pararectus incisions stand midway. In summary, the results of the present simulation provide full support for the clinical guidelines' recommendation to avoid midline incisions in abdominal surgeries whenever possible.

Keywords Incision, Abdominal wall, Open surgery, Laparotomy, Finite element method, Open-source software

Laparotomy is a common surgical procedure that has been used for diagnostic and therapeutic purposes in abdominal pathologies since the late nineteenth century[1]. One of the most usual complications following a laparotomy is incisional hernia (IH), which typically occurs within the first year after surgery, with a prevalence ranging from 9 to 20%[2]. However, incisional hernias have been reported to arise even up to 10 years post-surgery[2]. The incidence rate of IH has been reported to be notably dependent on the context of the laparotomy and/or patient characteristics[3]. The high prevalence and recurrence of IH have significant implications not only for patients' health[4,5] but also from an economic perspective[6,7]. Therefore the prevention of IH is of paramount importance. On the other hand, AW repair remains a complex surgical challenge, particularly in the context of preventing incisional hernias. In recent years, the concept of biomechanically calculated reconstruction (BCR) has emerged as an innovative method for enhancing hernia repair outcomes. Unlike standard reconstruction techniques, BCR uses mathematical formulas derived from experimental data to balance the forces acting on the abdominal wall and the retaining forces of reconstructed tissues[8]. Kallinowski et al.[9] contributed to this field by developing bench tests involving tissues, fixations, and textiles subjected to dynamic intermittent strain,

[1]Departament d'Enginyeria Informàtica i Matemàtiques, Universitat Rovira i Virgili, Av Països Catalans 26, Tarragona, Catalonia, Spain. [2]Abdominal Wall Surgery Unit, Department of General Surgery, Hospital Universitari Vall d'Hebron, Universitat Autònoma de Barcelona, Barcelona, Spain. [3]Departament d'Enginyeria Química, Universitat Rovira i Virgili, Av Països Catalans 26, Tarragona, Catalonia, Spain. ✉email: dolors.puigjaner@urv.cat

combined with low-dose computed tomography of the abdomen performed preoperatively. Furthermore, Nesse et al.[10] reported the effectiveness of BCR in a prospective cohort study on incisional hernias of different complexity.

Numerical finite element (FE) simulations have also significantly enhanced the understanding of the AW biomechanical behavior. A recent article by Spadoni et al.[11] provided a comprehensive review on numerical models and experimental techniques used to investigate AW biomechanics. This review cited relevant numerical studies that focused on either a passive[12] or an active[13,14] muscle response behavior, emphasizing how active muscle behavior allows simulations at higher intra-abdominal pressure (IAP) levels, such as those achieved during coughing or abdominal crunches. The review also highlighted the critical need for detailed experimental datasets to comprehensively validate FE models, which remains a persistent challenge for advancing biomechanical modeling in AW repair. In this respect, Todros et al.[15] proposed a FE model to evaluate the biomechanical aspects of laparoscopic hernia repair of AW muscles under various IAP conditions. Building upon this work, Todros et al.[14] developed a more advanced FE model which integrated the active muscle behavior and overcame the limitations of the simplified geometry used in their earlier model[13]. Jourdan et al.[16] conducted a sensitivity analysis exploring the impact of inter-individual variability on model outcomes. Using a simplified geometry, these authors investigated the passive inflation of the abdominal wall followed by muscular activation. Karrech et al.[17] applied fracture mechanics to study mechanical failure in the AW due to hernia-induced local damage while Aly[18] examined the influence of stoma aperture shape and mesh design on AW stress distribution, aiming to identify optimal mesh reinforcement designs.

The above-mentioned previous numerical studies exemplify both the increasing complexity and the future potential of FE simulations as a tool aimed to deepen the knowledge on AW repair. On the other hand, FE simulations can also provide valuable insights into the impact of surgical wounds (SW's) on the mechanical behavior of the abdominal wall. In two previous numerical studies, we investigated the AW mechanical response when subject to a level of intra-abdominal pressure (IAP) in the presence of either a stoma[19] or a trocar pattern characteristic of laparoscopy[20]. In the former study, we found that for a given IAP level the amount of trephine deformation strongly depended on the stoma location, with larger trephine shape changes occurring in laterally placed stomas. In our second previous study[20], we consistently found that laparoscopic wounds placed more laterally exhibited greater deformations. Moreover, we investigated the dependence of the SW deformation on the mechanical strength of its tissue[20]. The implied notion in this respect is that the strength level of a SW depends on its degree of healing, with a tender wound displaying strength levels much below the fully-healed value. Notwithstanding, we found that even in the worst case scenario (a very weak wound subject to an IAP as large as 20 kPa) the maximum SW volume change was within about 5%. This means, in practical terms, that the presence of a poorly healed laparoscopic wound would pose little threat to the AW mechanical integrity.

In the current study, we apply our previous methodology[20] to investigate the effects of much larger laparotomy incisions on the AW mechanics. The deformation of the wound tissue is analyzed for different locations and spatial orientations of the SW and, in each case, a wide range of the SW tissue stiffness is considered. More specifically, we consider five different incisions patterns located in different positions along the AW, each with a length ranging from 60 to 120 mm. In addition, we also analyze in each case the stress distribution experienced by the SW tissue and the muscle and/or aponeurotic tissues around it. We pay particular attention to the maximum stress levels within a tissue region in relation to its tensile strength limit. The occurrence of maximum stress levels surpassing the strength limit would be associated with a high risk of mechanical rupture of the tissue.

Our motivation is that the information provided by the present simulations can be valuable for surgeons in making decisions such as the location of the incision.

Models and methods

Geometry model

The geometry model used in this study is based on the model from our previous works[19,20]. As shown in Fig. 1, the model includes the linea alba (LA) and the following muscles: external oblique (EO), internal oblique (IO), rectus abdominis (RA), and transverse abdominis (TR). The model also considers the so-called rectus sheath (RS), which is formed by the aponeuroses of the EO, IO, and TR muscles. The RS is more fibrous than the regular muscular tissue. To account for this specificity, we defined three zones in the EO, IO, and TR muscles. The zone which we refer to as regular exhibits the typical characteristics of muscle tissue. The zone around the RA muscle represents the RS itself, that is, the aponeurotic tissue. In between these two zones, we define a thin intermediate transition region that exhibits a stiffness level midway that of the RS and the regular muscle.

We investigated five laparotomy incisions which are illustrated in Fig. 2. Specifically, we considered: (i) the most common midline incision[21], a vertical incision made on the LA (see Fig. 2a); (ii) a paramedian incision, a vertical incision made parallel to the midline incision and displaced to the left of the LA. (Fig. 2b); (iii) a pararectus incision, a vertical incision made parallel to the midline incision and located more to the left than the paramedian one (Fig. 2c); (iv) a transverse supraumbilical incision, a horizontal incision made above the RA muscle (Fig. 2d); (v) a subcostal incision (also known as Kocher incision), an oblique incision made at the right subcostal level (Fig. 2e). All the incisions were considered as surgical wounds post-surgery, that is, we assumed they were closed. Moreover, our model does not account for the effects of the suture. We therefore assume that either the suture has been already removed or, in the most common case of an absorbable material, the suture has completely degraded. The length, width, depth, surface area, and volume of each surgical wound are listed in Table 1.

Figure 3a–f display the muscles involved in each incision model. The midline incision (Fig. 3a) exclusively crosses the linea alba (LA). The paramedian (Fig. 3b) and the transverse supraumbilical (Fig. 3d) cut the RA muscle and the RS. The pararectus incision (Fig. 3c) was crafted taking care that it did not cut the regular tissue of any muscle; it averts the RA muscle and crosses the intermediate zone of the EO, IO and TR muscles. The

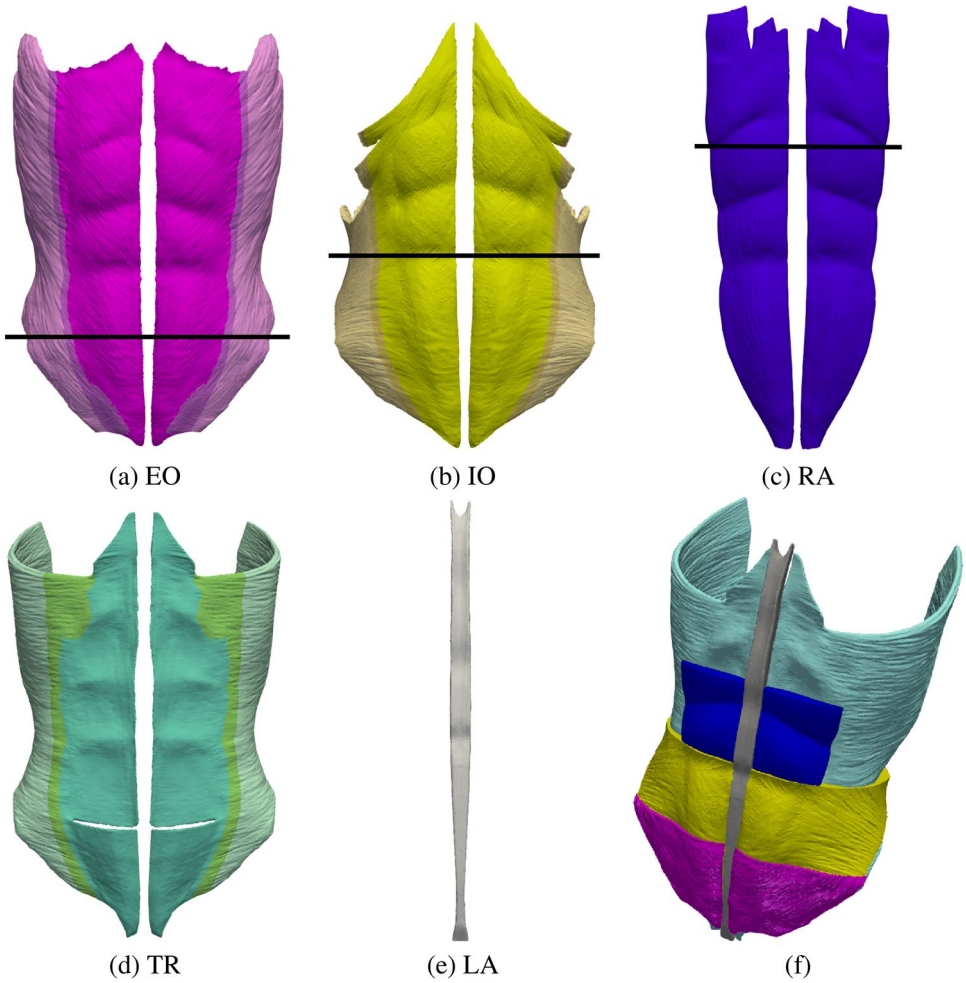

Fig. 1. Geometry model of the abdominal wall. The elements involved in the model are: (**a**) right and left external oblique muscles (EO), (**b**) right and left internal oblique muscles (IO), (**c**) right and left rectus abdominis muscles (RA), (**d**) right and left transverse abdominis muscles (TR) and (**e**) linea alba (LA). (**f**) View of the whole model. Note that as the involved muscles are superimposed only those muscle regions below black lines in parts (**a**)–(**c**) are displayed. In parts (**a**, **b**, **d**) the different regions (regular, intermediate transition, and aponeurotic muscle tissue) are denoted with increasingly saturated color tones.

subcostal incision (Fig. 3e) is the most complex one. Along most of its length (90 mm) it cuts the RA muscle and the RS. However, the most lateral section of the subcostal incision does not cross the RA but either the intermediate transition or the regular regions of the EO, IO and TR muscles.

Material properties

Following our prior research[19,20] we used an isotropic linear elastic model for the AW tissues

$$\boldsymbol{\sigma} = E\boldsymbol{\varepsilon} \tag{1}$$

where $\boldsymbol{\sigma}$ denotes the stress tensor, $\boldsymbol{\varepsilon}$ represents the strain tensor, capturing the relative deformation of tissues, and E is the elastic modulus, which takes a distinct value for each tissue. The E values assumed for each tissue, along with the corresponding bibliographic source, are summarized in Table 2.

A key point in the present study is how to characterize the mechanical behavior of the SW tissue. Both the regular muscle tissue and aponeurotic tissue are fibrous. These tissues are thus much stiffer (higher E values) than non-fibrous soft tissues are. As can be seen in Table 2, E values for regular muscles are typically above 0.1 MPa whereas the mechanical behavior of aponeurotic tissue is characterized by E values at least one order of magnitude higher. On the other hand, the elastic moduli of non-fibrous soft tissues are typically in the 1–10 kPa range[22].

Following surgery, the SW is sutured and its healing process begins. The healing of regular muscle and aponeurotic tissue is a very long process, in which the tissue progressively recovers its strength as fibers are progressively regenerated[23,24]. The suture is either removed or naturally degraded within a few weeks after surgery whereas it is known that the AW typically needs at least half a year to recover 70% of its original strength[23]. The

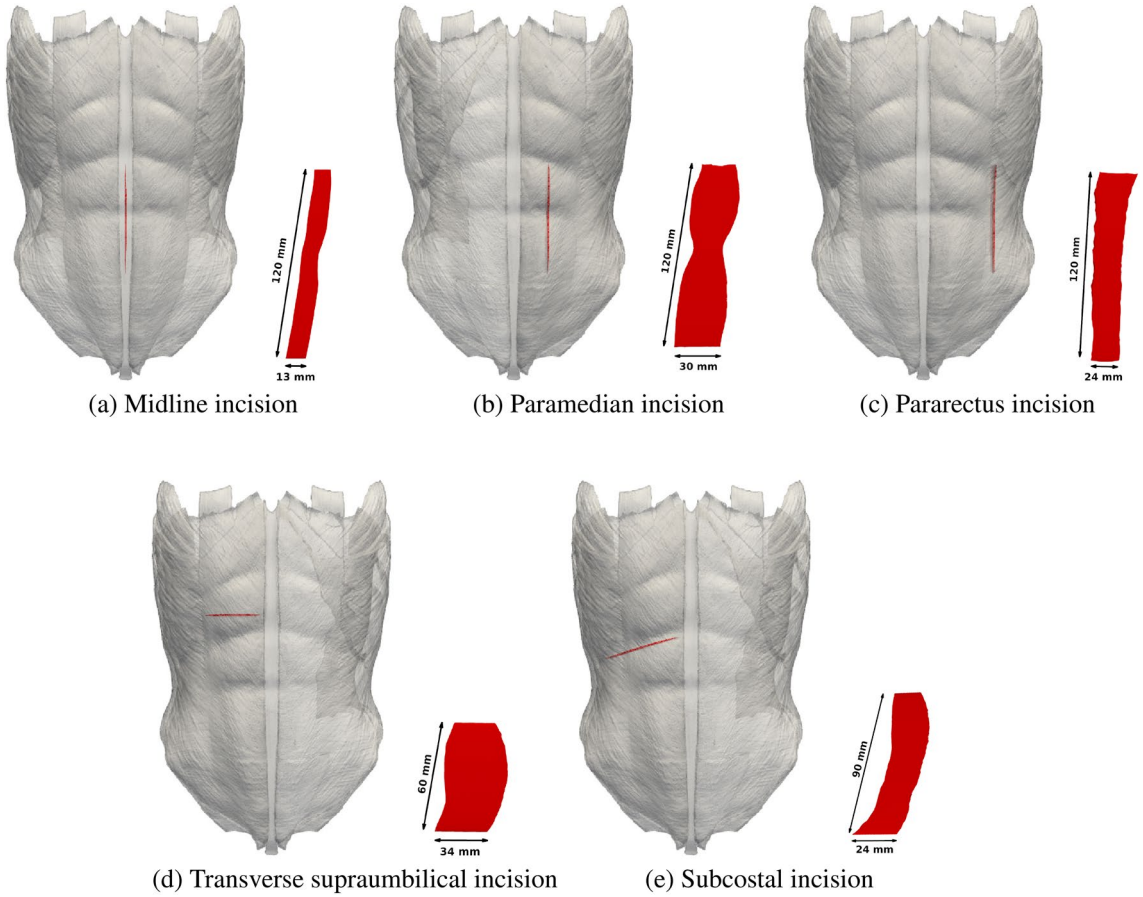

Fig. 2. Distribution and details of the incisions on the abdominal wall (AW) studied in this work, along with their lengths and depths. All incisions have a uniform width of 2 mm. (**a**) Midline incision model with a 120 mm-long vertical incision on the linea alba (LA), centered at the umbilicus. (**b**) Paramedian incision model with a 120 mm-long vertical incision parallel to and displaced to the left of the midline incision. (**c**) Pararectus incision model with a 120 mm-long vertical incision parallel to the midline incision, located more to the left than the paramedian incision. (**d**) Transverse supraumbilical incision model with a 60 mm-long horizontal incision located above the rectus abdominis muscle. (**e**) Subcostal incision model with a 90 mm-long oblique incision at the right subcostal level.

	Length (mm)	Width (mm)	Depth (mm)	Surface (cm^2)	Volume (cm^3)
Midline	120	2	13	32.78	2.27
Paramedian	120	2	30	71.12	5.26
Pararectus	120	2	24	48.39	3.45
Transverse supraumbilical	60	2	34	39.49	3.00
Subcostal	90	2	24	43.13	3.12

Table 1. Dimensions (length, width, depth), surface area, and volume for each of the five investigated laparotomy incisions.

focus in the present study is on how a SW that is ongoing healing, and already lacking suture support, reacts to an increase in IAP and how the AW mechanics is affected on the overall. The mechanical strength of the SW tissue will be characterized by the value of its elastic modulus, E_w. For a worst case scenario, when a SW suffers from a very poor healing and basically no fibers are being generated, we assumed $E_w = 10$ kPa (0.01 MPa). Numerical simulations were conducted across a broad spectrum of SW elastic modulus (E_w) values, ranging from 0.01 to 500 MPa. Values of E_w above the elastic modulus of the original tissue (prior to surgery) were used to simulate a scarred SW tissue. Although a highly stiff SW tissue is possible, its occurrence would be rare in practice.

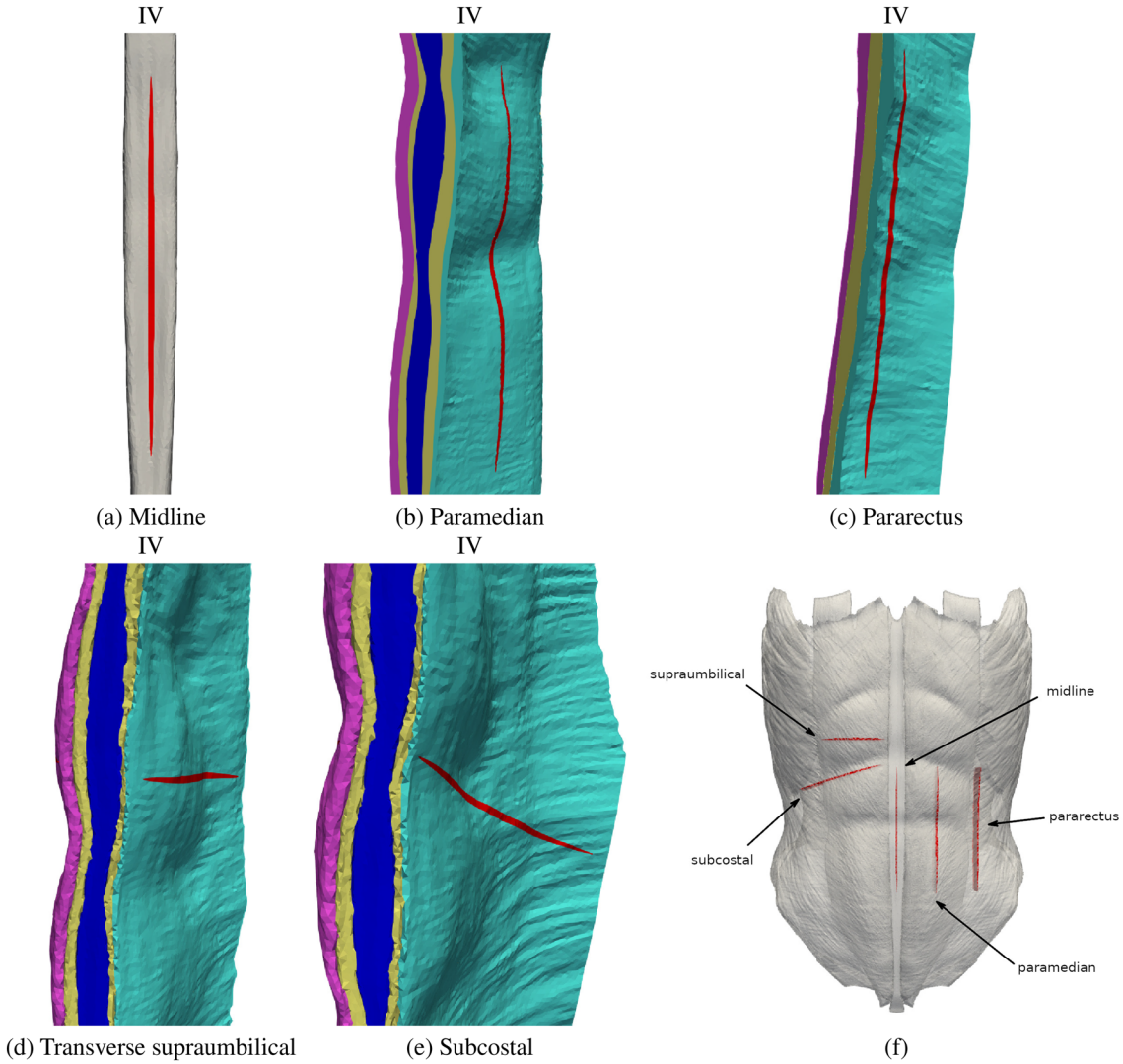

Fig. 3. Muscles involved in each laparotomy model (incisions highlighted in red): (**a**) midline incision, (**b**) paramedian incision, (**c**) pararectus incision, (**d**) transverse supraumbilical incision, and (**e**) subcostal incision. Muscles depicted include: EO (purple), IO (yellow), RA (blue), LA (grey), and TR (green). All views are inner views (IV), i.e. from the inside of the AW. A slight rotation was applied to better display the layers crossed by each incision. Figure (**f**) is included to show the location of all the incisions on the AW.

We assumed a Poisson ratio of $\eta = 0.4$ for surgical wounds[25] and $\eta = 0.49$ for the rest of tissues. The reported tensile strength values for the different tissues[26] are also included in Table 2. These values are useful for comparing with the stresses predicted by our simulations, allowing us to assess the potential risk of tissue rupture.

Numerical simulation

The FE simulations in this study were conducted using the Code Aster open source FE software[27]. A uniformly distributed intra-abdominal pressure (IAP) value was applied to the computational domain regions corresponding to the inner surface of the abdominal wall. Fixed zero deformation boundary conditions were set at the edges of the abdominal wall, where the muscles attach to the bones.

We imposed a strong continuity condition to model the contact between the different material elements. This simple contact model was indeed found to work well in our previous studies[19,20]. Note however that contact between contiguous layers of muscle and fascia was instead modeled as frictionless in some of the previously published simulations of AW mechanics[14]. Such a choice was aimed to characterize the relatively novel sliding behavior between fasciae and adjacent muscles[28], which is gaining attention within the research community.

For each specific geometry, simulations were performed for five uniformly distributed values of IAP, denoted as P_a. These values ranged from 4 to 20 kPa (30–150 mmHg), reflecting the normal IAP range during typical daily activities[29]. In all simulations, we calculated the distribution of the von Mises stress, σ_V, and the deformations along the abdominal wall (AW). The von Mises stress is a scalar index particularly suitable for failure analysis, allowing for a better interpretation of results[30]. In each case, we paid particular attention to

Tissue		E (MPa)	References	σ_{TS} (MPa)	References
RA		0.52	Cardoso[35]	0.23	Cardoso[35]
LA		72	Cooney et al.[37]	4.1	Hollinsky and Sandberg[26]
EO	Regular muscle	1	Cardoso[35]	0.57	Cardoso[35]
	Transition region	3.3			
	Rectus sheath	5.6	Ben Abdelounis et al.[36]	3.4	Hollinsky and Sandberg[26]
IO	Regular muscle	0.65	Cardoso[35]	0.39	Cardoso[35]
	Transition region	3.1			
	Rectus sheath	5.6	Ben Abdelounis et al.[36]	2.1	Hollinsky and Sandberg[26]
				3.4	
TR	Regular muscle	1.03	Cardoso[35]	0.73	Cardoso[35]
	Transition region	3.3			
	Rectus sheath	5.6	Ben Abdelounis et al.[36]	2.1	Hollinsky and Sandberg[26]

Table 2. Values of Young's modulus (E) and tensile strength (σ_{TS}) for the different tissues in our AW model. RA Rectus Abdominis, LA Linea Alba, EO Internal Oblique, IO Internal Oblique, TR Transverse Abdominis.

changes in the dimensions (surface and volume) of the surgical wounds, as well as the corresponding levels of stress they experienced, providing a qualitative indicator of the risk of tissue rupture.

Results and discussion

In this section, we present and analyze the results of our numerical simulations. The section is organized into three subsections: the first subsection details the impact of both IAP values and the stiffness of the wound tissue (E_w) on the deformation experienced by the abdominal wall; the second subsection focuses on the variations in dimensions (area and volume) of the surgical wounds (SW) as a function of E_w; and finally, the third subsection is dedicated to the levels of von Mises stress (σ_V) experienced by the muscles involved in each incision.

Abdominal wall deformation

Figure 4 shows the maximum deformation in the outward (ventral) direction, $\max \Delta_Y$, as a function of the applied IAP value, P_a, for various values of E_w and each of the investigated incisions. It can be seen that $\max \Delta_Y$ increases almost linearly with increasing P_a for any fixed value of E_w. Moreover, the effect of wound tissue stiffness E_w on $\max \Delta_Y$ depends on the wound's location. Figure 4 shows that for the paramedian, pararectus, and subcostal incisions increasing tissue stiffness to $E_w = 500$ MPa results in a decrease in $\max \Delta_Y$. In contrast, for the transverse supraumbilical and midline incisions, hardening the wound tissue to $E_w = 500$ MPa has minimal impact, particularly for the transverse supraumbilical incision, where the effect is negligible. It is important to note that the midline incision is located on the LA, a stiffer tissue compared to the muscular tissues where the other incisions are situated. Therefore, for the midline incision, $\max \Delta_Y$ values are compared to those obtained with $E_w = 72$ MPa, the Young's modulus of the LA. For the other incisions, comparisons are made with $E_w = 1$ MPa, a value close to the Young's modulus of muscular tissues.

Figure 4 further shows that softening the wound tissue to $E_w = 0.01$ MPa has a negligible effect on $\max \Delta_Y$ for the transverse supraumbilical incision. For the subcostal incision, this softening results in a very small but noticeable increase in $\max \Delta_Y$. On the contrary, the three vertical incisions (midline, paramedian, and pararectus) experience a considerable increase in deformation when the tissue becomes very soft ($E_w = 0.01$ MPa). This increase becomes more relevant as P_a rises. The midline incision exhibits the most significant increase, with $\max \Delta_Y$ levels reaching nearly 30 mm at the maximum pressure $P_a = 20$ kPa. Indeed, this incision is the only one that shows a notable increase in $\max \Delta_Y$ at $E_w = 0.1$ MPa. As the impact of softer tissue is more relevant in the vertical incisions (midline, paramedian, and pararectus), it is particularly interesting to examine the deformation Δ_Y across the entire abdominal wall for these three incisions. Figure 5 shows this deformation at the maximum pressure $P_a = 20$ kPa. For the midline incision, the abdominal wall exhibits significantly larger deformations around the wound compared to the reference case, even with $E_w = 0.1$ MPa. With $E_w = 0.01$ MPa, the deformation becomes higher, with Δ_Y values approaching 30 mm in some areas around the wound. This is consistent with the results displayed in Fig. 4. In contrast, with $E_w = 1$ MPa the overall AW deformation experience minimal changes compared to the reference case. Similarly, the paramedian and pararectus incisions with $E_w = 0.1$ MPa, display minimal differences from the reference case in overall abdominal wall behavior.

Figure 5e and g reveal that with $E_w = 0.01$, the global AW behavior for the paramedian and pararectus incisions is altered, showing orange areas in the central part of the abdomen, indicating deformations around 20 mm, in line with observations in Fig. 4. These figures also highlight a clear discontinuity in the distribution of Δ_Y around the wound. For the paramedian incision, there is a sudden transition from orange to yellow colors around the wound's central area, In the pararectus incision case, the transition is from yellow to greenish-blue. This discontinuity suggests that, although our linear model does not account for tissue rupture, the nonlinear effects in real-world scenarios would likely lead to tissue failure due to the stresses involved.

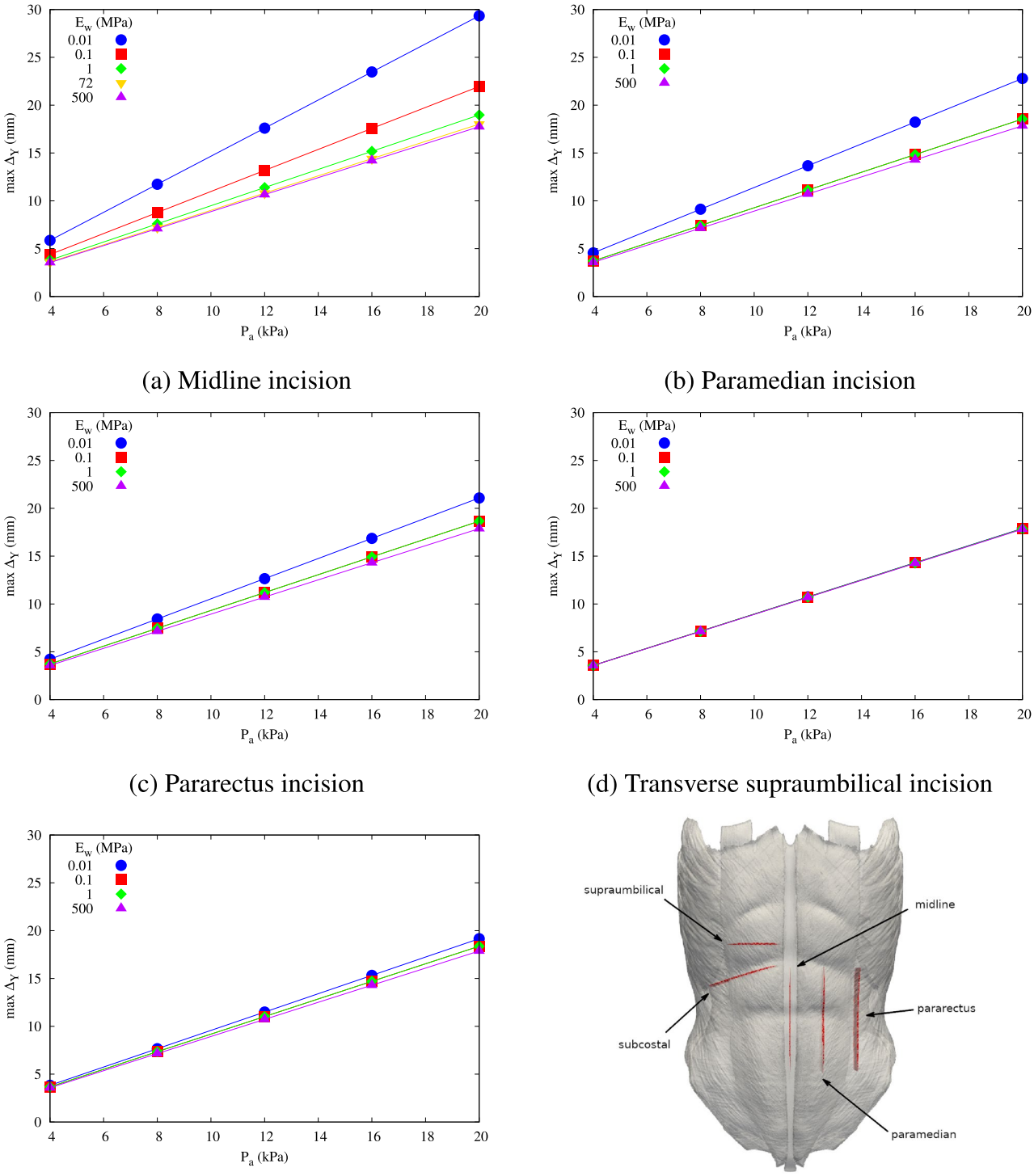

Fig. 4. Variation of the maximum deformation in the outward (ventral) direction, $\max \Delta_Y$, in the whole AW with the applied P_a level for four values of E_w, namely 0.01 MPa, 0.1 MPa, 1 MPa, and 500 MPa. (**a**) Midline, (**b**) paramedian, (**c**) pararectus, (**d**) transverse supraumbilical, and (**e**) subcostal. For the midline SW, the plot also includes $E_w = 72$ MPa, corresponding to the Young's modulus of the linea alba, as the SW is located along this tissue. Calculated values are marked with symbols, while the solid lines serve as a visual aid to suggest a hypothetical continuous trend. Figure (**f**) is included to show the location of all the incisions on the AW.

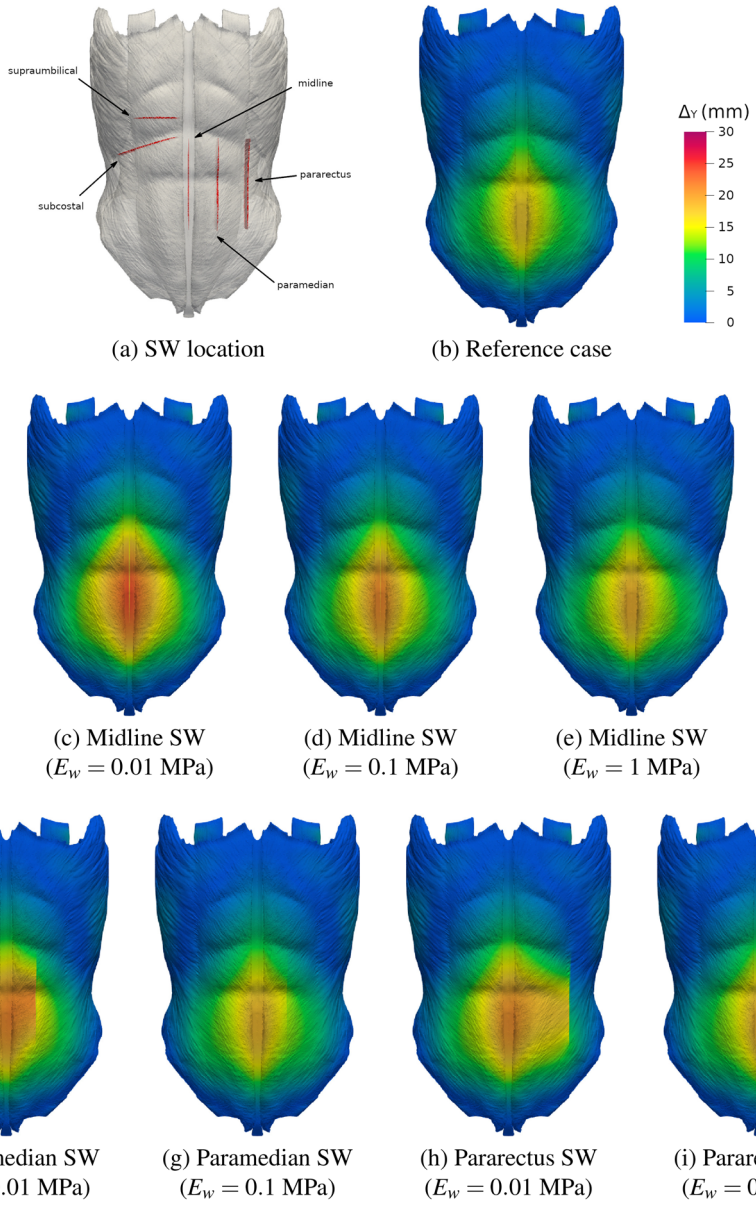

Fig. 5. Distribution of displacement Δ_Y in the outward (ventral) direction on the AW for $P_a = 20$ kPa. (**a**) location of all the incisions on the AW. (**b**) Reference case without incision. (**c**–**e**) Midline incision with E_w values of 0.01 MPa, 0.1 MPa, and 1 MPa, respectively. (**f**, **g**) Paramedian incision with E_w values of 0.01 MPa and 0.1 MPa, respectively. (**h**, **i**) Pararectus incision with E_w values of 0.01 MPa and 0.1 MPa, respectively. The scale used ranges from 0 to 30 mm for consistency with Fig. 4.

Surgical wound dimensions

Changes in the wound dimensions, specifically surface area and volume, can be computed using our numerical method. Since the predicted displacements of each computational node are available in the FE simulation output, we can calculate the corresponding changes in surface area and volume of the deformed SWs through numerical integration over the mesh elements-triangles for surface area and tetrahedra for volume. We denote V the volume of the deformed SW and V_0 the initial volume of the SW (see Table 1). Similarly, S represents the surface area of the deformed SW and S_0 the initial surface area of the SW. The relative variations in volume and surface area are then computed as V/V_0 and S/S_0, respectively.

In this section, we analyze the effect of varying the wound tissue stiffness, E_w on wound dimensions. Based on the findings from Section "Abdominal wall deformation", which indicated that the highest deformations occurred at the maximum pressure $P_a = 20$ kPa and that the vertical incisions (midline, paramedian, and pararectus) where the ones that deformed the most, we focus the analysis on these cases.

Figure 6 illustrates the relative changes in volume and surface area for the vertical incisions as a function of E_w. The figure shows that increasing tissue stiffness, even to a extreme value such as $E_w = 500$ MPa, has a negligible impact on changes in wound volume and surface area. This observation aligns with the results discussed

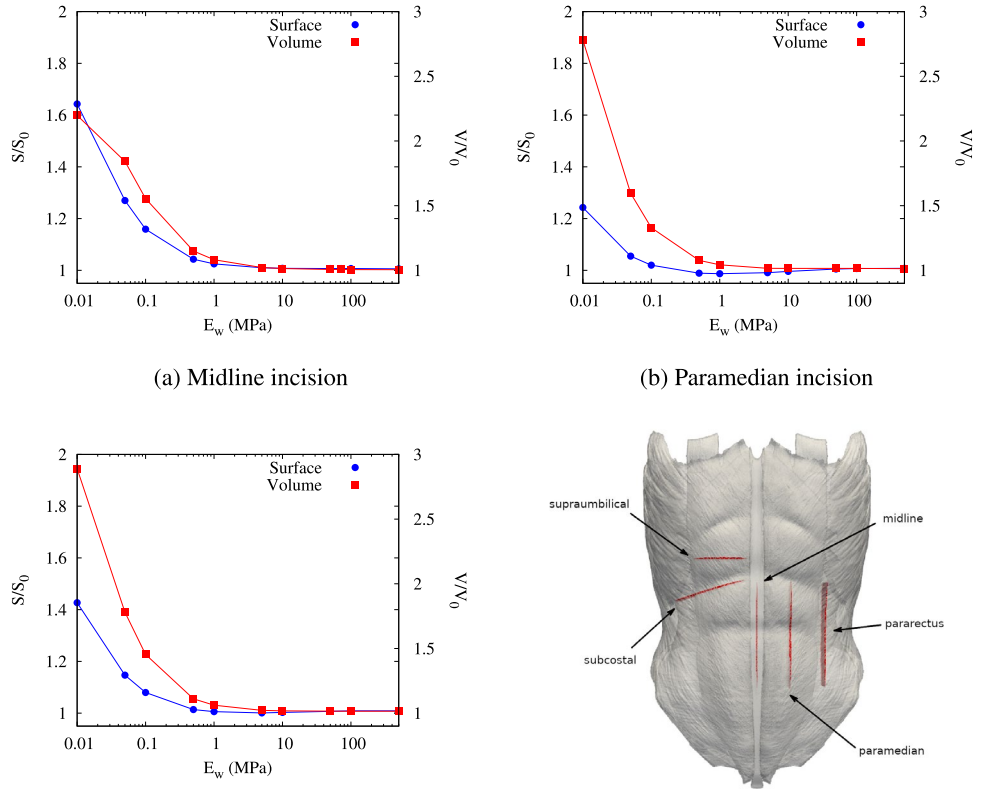

(a) Midline incision

(b) Paramedian incision

(c) Pararectus incision

(d)

Fig. 6. Relative change of surface area (S/S_0) and volume (V/V_0) when $P_a = 20$ kPa as a function of E_w for: (**a**) midline SW, (**b**) paramedian SW, and (**c**) pararectus SW. In these plots, calculated values are marked with symbols, while the solid lines provide a visual aid suggesting a hypothetical continuous trend. Subfigure (**d**) shows the distribution of all the incisions on the AW.

in Section "Abdominal wall deformation", which showed that hardening the tissue results in small deformation changes at high pressures (see Fig. 4). Conversely, when the tissue is softened, significant changes are observed, particularly in volume variation, although changes in surface area are also notable. For $E_w = 0.01$ MPa, the volume of the wound increases substantially: by approximately 190% for the pararectus incision, around 178% for the paramedian incision, and 120% for the midline incision. Surface area changes are also significant: around 64%, 43% and 24% for the midline, pararectus and paramedian incisions, respectively. When the tissue stiffness is reduced to $E_w = 0.1$ MPa, the variations in volume are more moderate, but still important. The volume increases by approximately 55% for the midline incision, 45% for the pararectus incision, and 33% for the paramedian incision. In this case, changes in surface area are quite modest: negligible for the paramedian incision, about 8% for the pararectus incision, and around 16% for the midline incision. It is important to note that the midline incision, situated on the LA, is surrounded by tissue that is significantly stiffer (Young's modulus $E = 72$ MPa) compared to the other two vertical incisions. Therefore, a reduction to $E_w = 0.1$ MPa in the midline case has a relatively more significant impact. This explains why the effects on the midline incision are more pronounced compared to the paramedian and pararectus incisions.

The substantial volume changes predicted for very soft SW tissue are consistent with the abdominal wall deformations discussed in Section "Abdominal wall deformation". The findings highlight a significant risk of tissue rupture for patients subjected to a high IAP of 20 kPa for prolonged periods. Such high IAP can be achieved during intense physical activities, such as jumping[29]. Our simulations underscore the vulnerability of abdominal tissues under these extreme conditions and emphasize the need for caution in patients with compromised wound tissues to prevent potential tissue rupture.

Von Mises stress distribution

An output from our simulations is the stress tensor within the tissues. From this stress tensor, we derive the von Mises stress (σ), a scalar value that can serve as an indicator of tissue failure risk. To evaluate this risk, we compare the von Mises stress with the reported experimental tensile strength (σ_{TS}) of each tissue (see Table 2). In this section, we analyze how varying the wound tissue stiffness (E_w) affects the von Mises stress distribution on the muscles involved in the incision. Our focus is on the three vertical incisions for the highest IAP value of $P_a = 20$ kPa.

The midline incision intersects only the LA, as illustrated in Fig. 7a. Figure 7b presents the von Mises stress distribution on the LA for the reference case with $P_a = 20$ kPa. Simulations not included in the figure revealed that reducing P_a to 16 kPa results in minimal changes in the von Mises stress distribution on the LA. Additionally, simulations demonstrated that when the midline incision has $E_w = 72$ MPa, a value matching the elastic modulus of the LA, the stress distribution on the LA remains unchanged from the reference case. In the reference scenario, red areas are observed on the inner side of the LA in the inguinal region (the lower part of the figure), indicating stress values exceeding 4 MPa, which surpass the tensile strength of the LA (see Table 2). These results suggest that even in the absence of an incision, an individual exposed to abdominal pressures above 16 kPa for extended periods might be at risk of tissue rupture. When the tissue in the midline wound is very soft ($E_w = 0.01$ MPa), new high-stress regions emerge, particularly at both the upper and lower ends of the wound on the outer side (OV), as shown in Fig. 7c. These high stress area are typical of situations where tissues with very different elastic moduli (LA ans soft SW in our case) are in contact, as the stiffer tissue must accommodate the more deformable softer tissue. For very hard tissue ($E_w = 500$ MPa), new stress areas exceeding 4 MPa arise only within the wound itself (Fig. 7d). However, since very rigid materials are expected to have high tensile strength, the risk of rupture remains minimal. Therefore, our results indicate an increased risk of tissue failure when the midline wound has a very low E_w, underscoring the need to avoid excessive physical activity in such cases. It should be noted that some everyday activities such as coughing are often unavoidable. As an example, in one instance it was reported that approximately one third of the patients undergoing abdominal surgery coughed at least 425 times in the first 24 h postoperatively[9].

The paramedian incision involves four muscles: the EO, IO, TR, and RA, as shown in Fig. 8a. Note that for the EO, IO and TR the paramedian incision only involves the part of the tissue corresponding to the rectus sheath. Figure 8b–d display the von Mises stress distribution for the reference, case as well as for cases with a paramedian incision where $E_w = 0.01$ MPa and $E_w = 500$ MPa, all under the highest IAP, $P_a = 20$ kPa. In these figures, the outside view (OV) shows the von Mises stress on the rectus sheath part of the EO, whereas the inside view (IV) displays the stress on the rectus sheath part of the TR muscle. The color scale ranges from 0 to 2 MPa, focusing on whether the stress exceeds the tensile strength (σ_{TS}) of the tissue, which ranges from 2.1 to 3.4 MPa for the rectus sheath (see Table 2). Figure 8b–d reveal that variations in E_w have minimal effect on the von Mises stress distribution on the EO (OV) or TR (IV). Both the reference case and the soft tissue case ($E_w = 0.01$ MPa) lack red zones, indicating that stress values do not exceed the σ_{TS} for the rectus sheath and thus there is no risk of tissue failure. With very stiff SW tissue ($E_w = 500$ MPa), the incision area appears predominantly red, indicating stress levels above 2 MPa. However, as previously mentioned for the midline incision, very stiff tissue can endure high stresses without significant risk of rupture.

Figure 8e–h focus on the RA muscle, which is not part of the rectus sheath and is not visible in Fig. 8b–d because it is between other muscles. These figures illustrate the von Mises stress distribution for the RA muscle with a SW tissue stiffness of $E_w = 0.01$ MPa, varying the intra-abdominal pressure (P_a) from 20 to 8 kPa in 4 kPa decrements. Regions where the von Mises stress exceeds the tensile strength of the RA (0.23 MPa) are highlighted in pink. The analysis of these figures reveals that, regardless of P_a, the entire contact area between the RA and the LA exceeds 0.23 MPa, reflecting the interaction between tissues with significantly different elastic moduli-the LA being stiffer and the RA much softer. At $P_a = 20$ kPa, a pressure level that could occur during a physical activities such as jumping[29], substantial pink areas are observed at both ends of the wound, indicating significant stress at these locations. Furthermore at $P_a = 20$ kPa, additional pink patches emerge in other regions of the RA, not directly related to tissue contact with differing moduli. As P_a decreases to 16 kPa, these regions become smaller but remain evident. At $P_a = 12$ kPa, the pink zones at the upper and lower ends of the wound diminish considerably, and at $P_a = 8$ kPa, only the contact area between the LA and RA remains

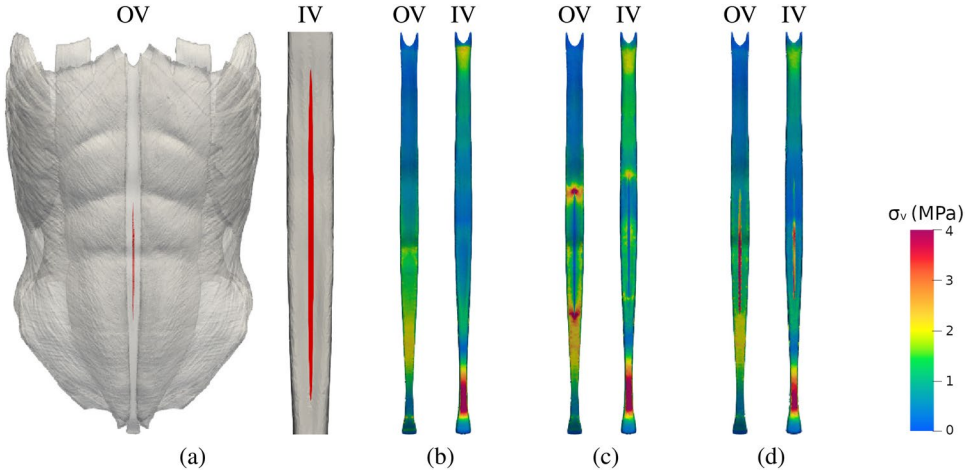

Fig. 7. Midline incision. (**a**) SW location and involved muscles: LA (grey). (**b–d**) Outside view (OV) and inside view (IV) of the Von Mises stress distribution. (**b**) LA for the reference case model (without incision). (**c**) LA and midline incision with $E_w = 0.01$ MPa. (**d**) LA and midline incision with $E_w = 500$ MPa. The applied pressure was $P_a = 20$ kPa in all cases.

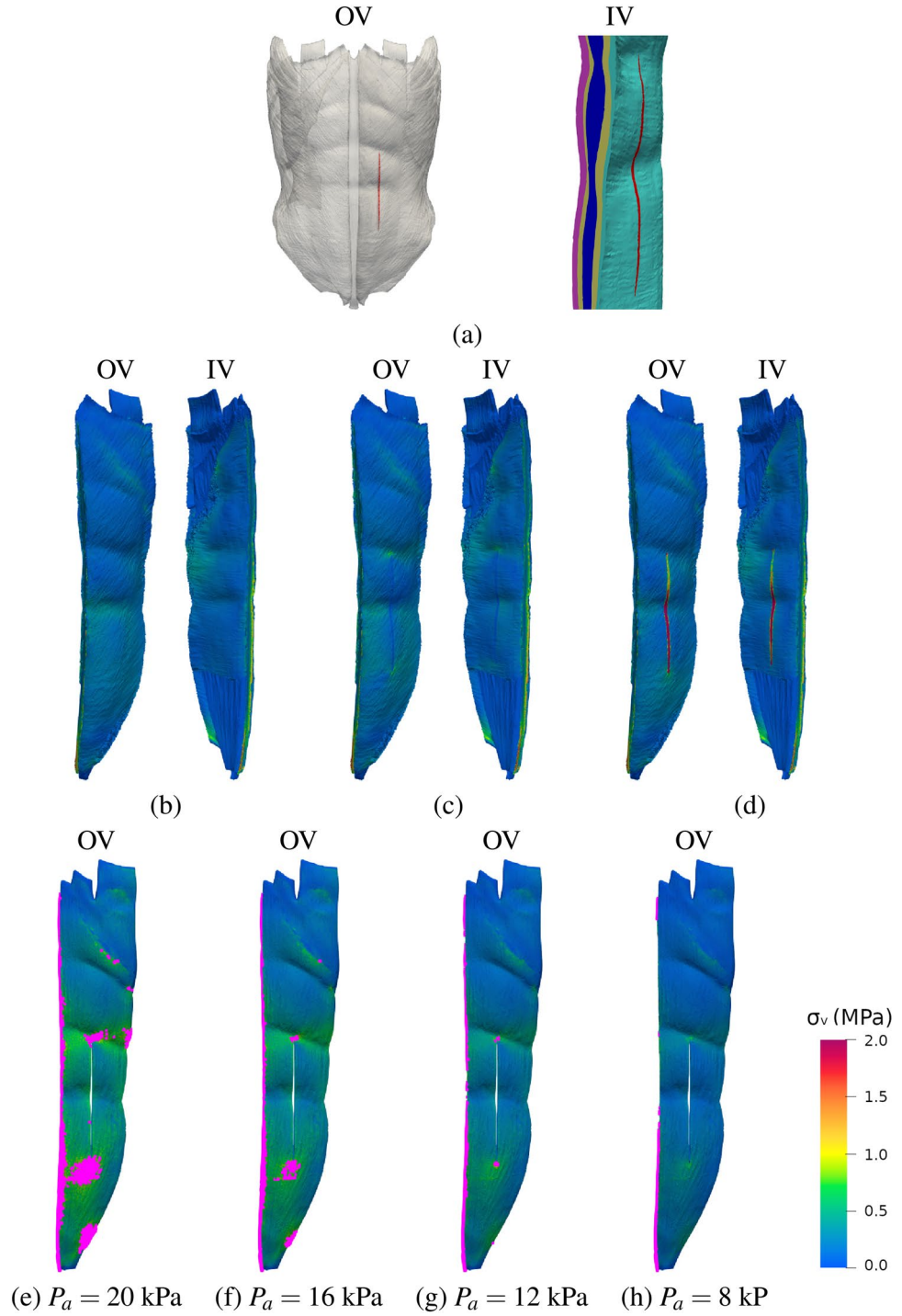

Fig. 8. Paramedian incision. (**a**) SW location and involved muscles: EO (purple), IO (yellow), RA (blue), and TR (green). (**b**–**d**) Outside view (OV) and inside view (IV) of the Von Mises stress distribution in the region around the incision with $P_a = 20$ kPa. (**b**) Reference case. (**c**) Paramedian incision with $E_w = 0.01$ MPa. (**d**) Paramedian incision with $E_w = 500$ MPa. (**e**–**h**) Outside view of the Von Mises stress distribution on the RA muscle with $E_w = 0.01$ MPa and different P_a values. Regions exceeding the tensile strength for RA $\sigma_{TS} = 0.23$ MPa are colored in pink. The P_a values are within the range reported by Cobb et al.[29], corresponding to the following maneuvers: (**e**) jumping, (**f**) standing coughing, (**g**) coughing and (**h**) standing Valsalva.

highlighted in pink. Values of P_a of 16 and 12 kPa can be reached during activities such as standing or coughing, respectively[29]. Thus, for the paramedian incision, a very soft wound tissue is relatively safe in terms of rupture risk, provided the patient does not engage in intense physical activities like jumping or squats[29,31].

The pararectus incision involves three muscles: the EO, IO, and TR, as shown in Fig. 9a. Since the incision is performed in the transition zone of these muscles, the adjacent tissue comprises either the rectus sheath or the transition zone tissue. Figure 9 illustrates the von Mises stress distribution on these muscles under the highest IAP, $P_a = 20$ kPa. Specifically, Fig. 9b–d display the von Mises stress distribution on the EO (OV) and the

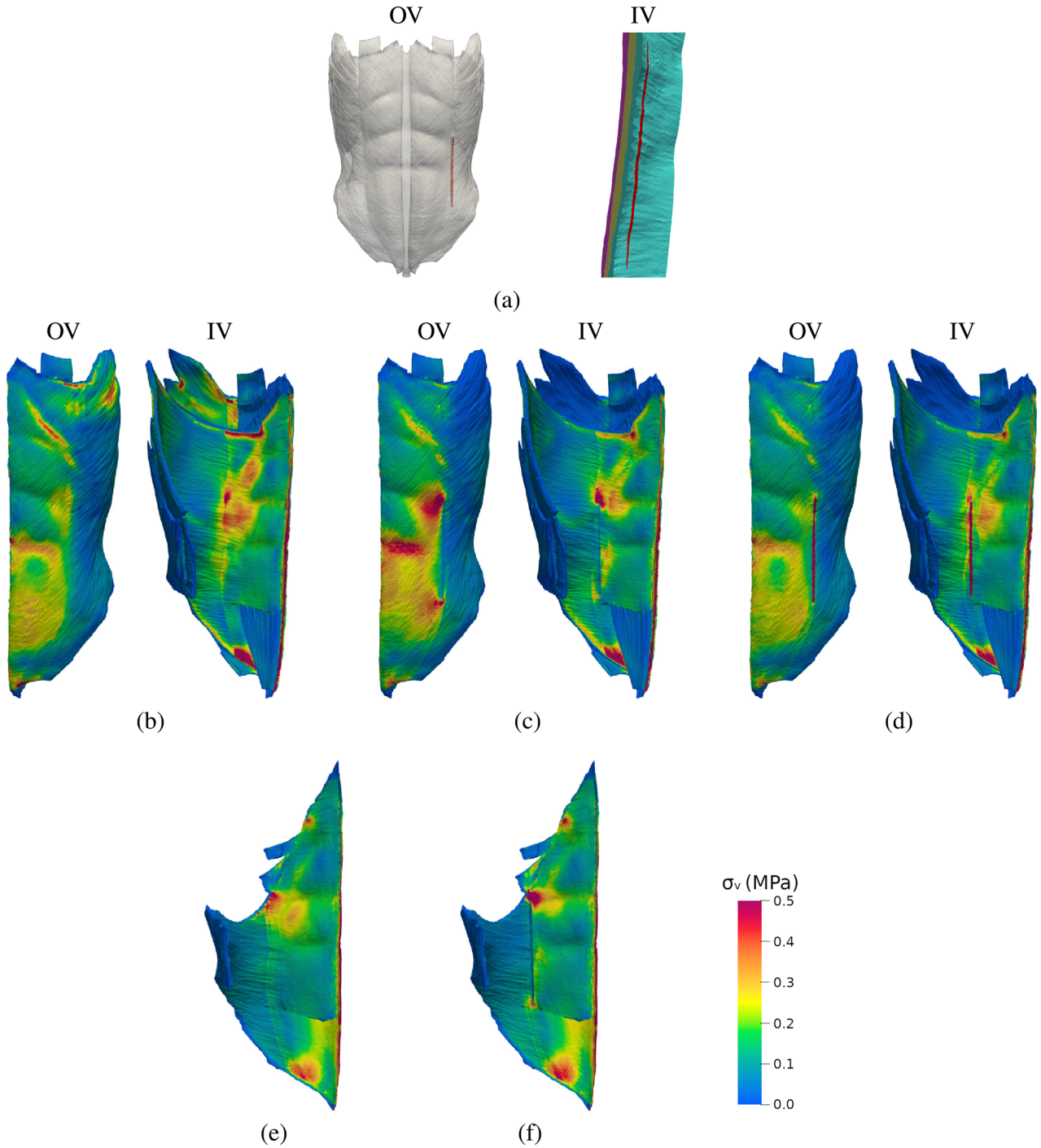

Fig. 9. Pararectus incision. (**a**) SW location and involved muscles: EO (purple), IO (yellow) and TR (green). (**b**–**d**) Outside view (OV) and inside view (IV) of the Von Mises stress distribution in the region around the incision. (**b**) Reference case. (**c**) Pararectus incision with $E_w = 0.01$ MPa. (**d**) Pararectus incision with $E_w = 500$ MPa. (**e**, **f**) Inside view of the Von Mises stress distribution on the IO muscle. (**e**) Reference case. (**f**) Pararectus incision with $E_w = 0.01$ MPa. The applied pressure was $P_a = 20$ kPa in all cases.

TR (IV) for the reference case as well as for a pararectus incision with $E_w = 0.01$ MPa and $E_w = 500$ MPa. The stress distribution on the inside part of the IO for the reference case and $E_w = 0.01$ MPa is shown in Fig. 9e–f. Figure 9d illustrates that, similar to the other incisions studied, when the wound tissue is very stiff ($E_w = 500$ MPa), the primary change compared to the reference case is the significantly increased stress within the wound itself (indicated by red areas on both the internal and external sides). However, as previously noted, these high stress levels do not pose a rupture risk due to the high tensile strength of very stiff tissues. For very soft wound tissue ($E_w = 0.01$ MPa), significant differences from the reference case are observed primarily on the external side. High-stress zones emerge on the EO near the superior and inferior ends of the wound, extending towards the rectus sheath region of the EO (shown to the left in Fig. 9c). In contrast, changes in stress on the TR (see Fig. 9b,c) and IO (see Fig. 9e,f) are minor. It is important to note that all high-stress zones are located in regions where the tissue is not regular muscle but transition zone, which has a higher Young's modulus. Consequently, these high-stress zones do not pose a failure risk, as they remain below the tensile strength of the transition tissue.

Figures not included here showed that, for both transverse supraumbilical and subcostal incisions, the presence of SW does not significantly affect the stress distribution in the surrounding muscles, regardless of the stiffness of the SW tissue.

It is insightful to focus on the wound itself and to analyze how the maximum stress ($\sigma_{\max}$) sustained by the wound varies with the stiffness of the wound tissue (E_w), as illustrated in Fig. 10. This figure also includes the $\sigma_{\max}$ evolution for the LA in the midline incision case and for the RA and IO in the other incision types. It is seen that, in all cases, when the wound becomes significantly stiffer than the surrounding tissues, the $\sigma_{\max}$ sustained by the wound increases, even surpassing the maximum stress supported by the RA and IO, or the LA. Note that $\sigma_{\max}$ for the LA, RA and IO also tends to rise with increasing E_w values, with the sole exception of the IO in the pararectus incision. The increase in $\sigma_{\max}$ in the wound is expected, as stiffer tissue provides greater resistance to deformation compared to the softer surrounding tissue.

The most interesting observation arises when E_w is reduced. As the wound tissue becomes excessively soft, the stress in the wound tends to increase, posing a clear risk of rupture. Among the investigated incisions, the transverse supraumbilical incision exhibits the least risk of rupture with SW tissue, reaching a $\sigma_{\max}$ of about 0.5 MPa at the extreme $E_w = 0.01$, a $\sigma_{\max}$ value which roughly double the maximum stress achieved at $E_w = 1$. The subcostal, paramedian, and pararectus incisions show similar $\sigma_{\max}$ values for $E_w = 0.01$, which are all around 1.6 MPa, indicating comparable rupture risks at this stiffness level. While for the subcostal and pararectus incisions, $\sigma_{\max}$ doubles at $E_w = 0.01$ compared to $E_w = 1$, the paramedian incision does not exhibit this doubling until E_w decreases to 0.05. The midline incision demonstrates the highest $\sigma_{\max}$ values, beginning to increase at $E_w = 0.5$ and reaching values close to 11 MPa at $E_w = 0.01$. Therefore, in terms of the risk of rupture for the wound tissue itself, our results indicate that the safest wound type is the transverse supraumbilical incision, while the midline incision is, by far, the least safe.

Study limitations

The main limitation of this study is the absence of clinical data to validate our numerical results. Computed tomography (CT) imaging at rest and during the Valsalva maneuver has shown large interindividual variation, with differences in tissue distension reaching up to 18-fold (see Table 1 in Kallinowski et al.[9]). Our current simulations did not account for this significant variability. A systematic recollection of clinical data would provide the basis for devising patient-specific simulations of AW mechanics that would account for the significant variability among patients. Biomechanically calculated reconstructions[9] might also be helpful in the future design of patient-specific simulations on a laparotomy surgery postoperative

Another potential limitation concerns the characteristics of the mathematical model we employed. Given the fibrous nature of muscles and aponeurosis, hyper-elastic non-isotropic constitutive models have been often used in numerical simulations of AW mechanics[11,16,32,33]. In the present study, we assumed instead the linear elastic isotropic constitutive model for all AW tissues, which is a reasonable choice provided that large deformations are not considered in the simulations[20]. Our choice of linear elasticity however forced us to restrict the present simulations to IAP values not larger than 20 kPa (150 mm Hg). Thus, we could not simulate the AW response in patients undergoing intense activity such as a severe coughing, jumping or squats, for which IAP levels in the 200–300 mm Hg range have been reported[29,31].

There is a second more subtle limitation inherent to the use of either linear elastic or hyperelastic constitutive models for the AW tissues. These elastic models assume reversibility, that is, the tissue always recovers its original state when the loading it has been subjected to is released. Thus, elastic models are not apt to simulate the effects of cyclic loadings, as would be the case for example in postoperative laparotomy patients undergoing repetitive exercising, or simply suffering high frequency coughing episodes. It should be noted that cyclic loadings are considered within cutting-edge studies to enhance AW reconstruction techniques[10] and optimize the design of standardized sutures[34].

We prescribed the values of the Young modulus of the different AW tissues according to the experimental works reported by Cardoso[35], Ben Abdelounis et al.[36] and Cooney et al.[37], which were respectively published in 2012, 2013 and 2016 (see Table 2). In a more recent study, Kriener et al.[38] characterized the tensile properties of the tissues that comprise the human abdominal wall by means of uniaxial testing on fresh-frozen and fresh-never-frozen tissue samples. Kriener et al.[38] reported E values for the EO, IO, TA and RA muscles that closely aligned with the ones previously published by Cardoso[35]. Similarly, values of the Young modulus for the rectus sheath measured by Kriener et al. were consistent with the mean value reported by Ben Abdelounis et al.[36]. For the LA, Kriener et al. reported E values that fell within the wide range (8–72 MPa) reported by Cooney et al.[37] even though they tended toward the lower end. Note that in our simulations we selected instead the upper bound of this experimental range ($E = 72$ MPa for the LA). Additionally, we note a potential bias in experimental

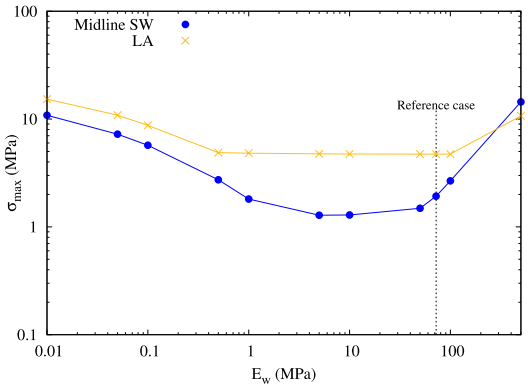

(a) Midline

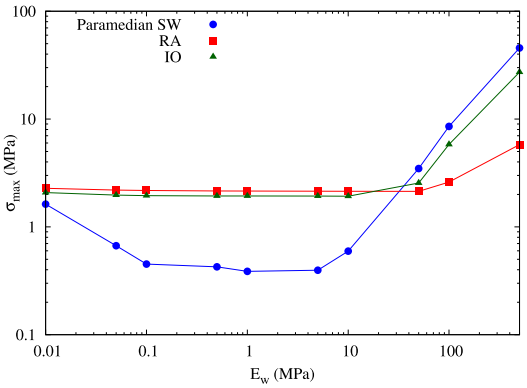

(b) Paramedian

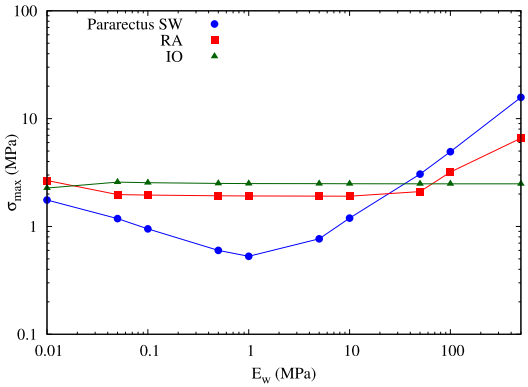

(c) Pararectus

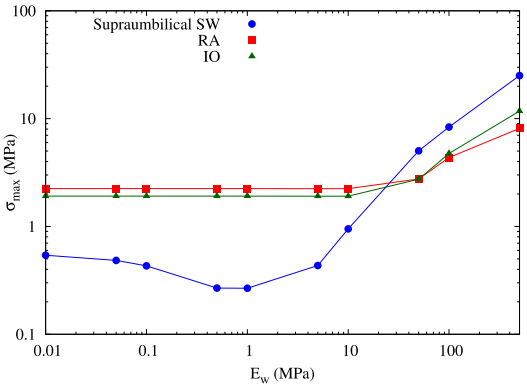

(d) Transverse supraumbilical

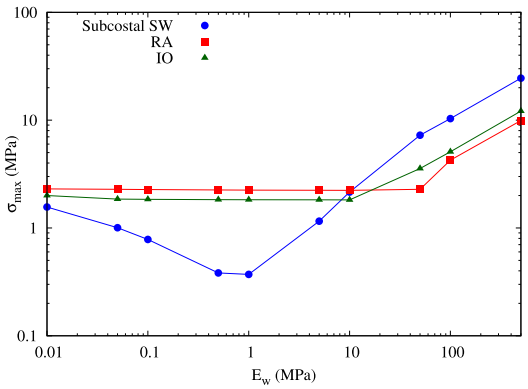

(e) Subcostal

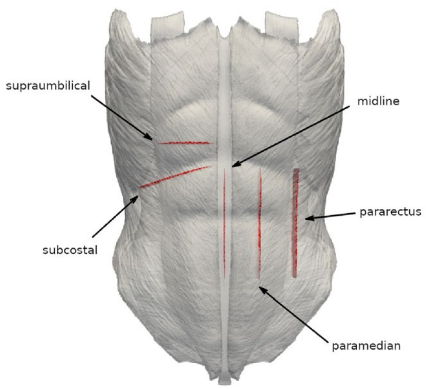

(f)

Fig. 10. Dependence of the maximum von Mises stress ($\sigma_{\max}$) on E_w when an IAP of 20 kPa is applied for: (**a**) the midline SW and LA tissues; (**b**) the paramedian SW, RA, and IO tissues; (**c**) the pararectus SW, RA, and IO tissues; (**d**) the transverse supraumbilical SW, RA, and IO tissues; (**e**) the subcostal SW, RA, and IO tissues. In these plots, calculated values are marked with symbols, while solid lines provide a visual aid to suggest a hypothetical continuous trend. Subfigure (**f**) shows the distribution of all the incisions on the AW.

studies as most tissue samples are typically obtained from elderly donors who are more likely to suffer from underlying pathologies, a fact that might inflate stiffness measurements[38].

Laparotomy lengths in clinical practice may vary significantly depending on the type of surgical procedure. In this study, we focused on a single incision length, which we considered intermediate between small and large laparotomy incisions and consistent across all studied laparotomy locations. Moreover, this study considered only the supine posture. The influence of laparotomy length[39], posture (e.g., sitting, standing)[40] and variations in cranio-caudal positioning of the incision on abdominal wall mechanics were not analyzed. These factors should be addressed in future research to provide a more comprehensive understanding of abdominal wall mechanics.

Advanced models, such as the one proposed by Yousefi et al.[41] which incorporates the wound healing process following the closure of a midline laparotomy incision, are available in the literature. Although the implementation of such a more comprehensive mathematical model is beyond the scope of the current study, it should be noted that our results regarding the midline laparotomy incision align with the findings of Yousefi et al.[41].

Conclusions

To the best of our knowledge, our study is the first to analyze several types of abdominal wall incisions commonly used in surgical practice other than the midline laparotomy. Current simulation results revealed that the stiffness of surgical wound tissue (E_w) significantly influences the deformation of the abdominal wall, with the location of the incision playing a crucial role. Vertical incisions, including midline, paramedian, and pararectus, exhibit higher sensitivity to changes in E_w, particularly when the tissue is very soft. The midline incision is particularly prone to increased deformation under high intra-abdominal pressure (IAP) when E_w is reduced. Results also indicates that softening the tissue results in substantial increments in the wound dimensions, especially in volume. This result align with observed abdominal wall deformations and underscore the potential risks associated with high intra-abdominal pressures for low E_w. Furhermore, very soft tissue ($E_w = 0.01$ MPa) increases the von Mises stress in the surrounding muscles of the incision, particularly around the wound. The achieved high stress may result in a clear risk of tissue rupture, especially for the midline incision. Conversely, very stiff tissue ($E_w = 500$ MPa) has a negligible impact on both abdominal wall deformation and wound volume and surface area. Regarding the stress distribution, a very stiff wound tissue results in high stress within the wound itself. Despite this, the increased stress generally remains within the tissue's tensile strength, avoiding, thus, the risk of rupture.

On overall it may be concluded that the transverse supraumbilical incision presents the lowest risk of rupture, making it the safest choice among the incisions studied. The midline and paramedian incisions are the most vulnerable, with the midline incision experiencing the greatest deformation under high intra-abdominal pressure and the paramedian incision showing the highest risk of rupture based on von Mises stress (VMIS) analysis. The pararectus and subcostal incisions present intermediate risks: the pararectus incision, while deforming more than the subcostal, demonstrates a lower risk of rupture according to VMIS, as it only crosses the rectus sheath. Meanwhile, the subcostal incision, although slightly less secure than the transverse supraumbilical due to marginally greater deformations, still offers a reasonable compromise between safety and surgical feasibility. Note that the practical use of the transverse supraumbilical incision may be limited by its shorter length, constrained by the ribcage.

In summary, the analysis of alternative laparotomy incisions represents a strength of our research, enabling us to compare different techniques for abdominal access while reinforcing our findings with the recent updates to clinical guidelines for abdominal wall closure published by the European and American Hernia Societies[42]. Our in silico findings are aligned with these guidelines, which recommend avoiding midline incisions in the abdominal wall to reduce the risk of incisional hernia.

Data availability

The datasets used and/or analyzed during the current study are available from the corresponding author on reasonable request.

Received: 16 October 2024; Accepted: 15 May 2025
Published online: 26 May 2025

References

1. Atkins, K., Schneider, A. & Charles, A. Negative laparotomy rates and outcomes following blunt traumatic injury in the united states. *Injury* **54**, 110894. https://doi.org/10.1016/j.injury.2023.110894 (2023).
2. Diener, M. K., Voss, S., Jensen, K., Büchler, M. W. & Seiler, C. M. Elective midline laparotomy closure: The inline systematic review and meta-analysis. *Ann. Surg.* **251**, 843–856. https://doi.org/10.1097/SLA.0b013e3181d973e4 (2010).
3. Pereira-Rodríguez, J. A., Bravo-Salva, A., Argudo-Aguirre, N., Amador-Gil, S. & Pera-Román, M. Defining high-risk patients suitable for incisional hernia prevention. *J. Abdom. Surg.* **2**, 6. https://doi.org/10.3389/jaws.2023.10899 (2023).
4. van Ramshorst, G. H., Eker, H. H., Hop, W. C., Jeekel, J. & Lange, J. F. Impact of incisional hernia on health-related quality of life and body image: A prospective cohort study. *Am. J. Surg.* **204**, 144–150. https://doi.org/10.1016/j.amjsurg.2012.01.012 (2012).
5. van Ramshorst, G. H., Eker, H. H., van der Voet, J. A., Jeekel, J. & Lange, J. F. Long-term outcome study in patients with abdominal wound dehiscence: A comparative study on quality of life, body image, and incisional hernia. *J. Gastrointest. Surg.* **17**, 1477–1484 (2013).
6. Rutkow, I. M. Demographic and socioeconomic aspects of hernia repair in the united states in 2003. *Surg. Clin.* **83**, 1045–1051. https://doi.org/10.1016/S0039-6109(03)00132-4 (2003).
7. Gillion, J., Sanders, D., Miserez, M. & Muysoms, F. The economic burden of incisional ventral hernia repair: A multi-centric cost analysis. *Hernia* **20**, 819–830. https://doi.org/10.1007/s10029-016-1480-z (2016).
8. Lesch, C. et al. Stronghold first-year results of biomechanically calculated abdominal wall repair: A propensity score matching. *Hernia* **28**, 63–73. https://doi.org/10.1007/s10029-023-02897-7 (2024).

9. Kallinowski, F. et al. The grip concept of incisional hernia repair-dynamic bench test, CT abdomen with Valsalva and 1-year clinical results. *Front. Surg.* **8**, 602181. https://doi.org/10.3389/fsurg.2021.602181 (2021).
10. Nessel, R., Löffler, T., Rinn, J. & Kallinowski, F. Three-year follow-up of the grip concept: An open, prospective, observational registry study on biomechanically calculated abdominal wall repair for complex incisional hernias. *Hernia* **28**, 913–924. https://doi.org/10.1007/s10029-024-03064-2 (2024).
11. Spadoni, S., Todros, S. & Pavan, P. G. Numerical modeling of the abdominal wall biomechanics and experimental analysis for model validation. *Front. Bioeng. Biotechnol.* **12**, 1472509. https://doi.org/10.3389/fbioe.2024.1472509 (2024).
12. Pachera, P. et al. A numerical investigation of the healthy abdominal wall structures. *J. Biomech.* **49**, 1818–1823. https://doi.org/10.1016/j.jbiomech.2016.04.019 (2016).
13. Pavan, P. G., Todros, S., Pachera, P., Pianigiani, S. & Natali, A. N. The effects of the muscular contraction on the abdominal biomechanics: A numerical investigation. *Comput. Methods Biomech. Biomed. Eng.* **22**, 139–148. https://doi.org/10.1080/10255842.2018.1540695 (2019).
14. Todros, S., de Cesare, N., Concheri, G., Natali, A. N. & Pavan, P. G. Numerical modelling of abdominal wall mechanics: The role of muscular contraction and intra-abdominal pressure. *J. Mech. Behav. Biomed. Mater.* **103**, 103578. https://doi.org/10.1016/j.jmbbm.2019.103578 (2020).
15. Todros, S. et al. Computational modeling of abdominal hernia laparoscopic repair with a surgical mesh. *Int. J. Comput. Assist. Radiol. Surg.* **13**, 73–81. https://doi.org/10.1007/s11548-017-1681-7 (2018).
16. Jourdan, A. et al. Numerical investigation of a finite element abdominal wall model during breathing and muscular contraction. *Comput. Methods Programs Biomed.* **244**, 107985. https://doi.org/10.1016/j.cmpb.2023.107985 (2024).
17. Karrech, A., Ahmad, H. & Hamdorf, J. M. Biomechanical stability of hernia-damaged abdominal walls. *Sci. Rep.* **130**, 4936. https://doi.org/10.1038/s41598-023-31674-w (2023).
18. Aly, O. E. Addressing parastomal herniation through biomechanical simulation. *Hernia* **27**, 565–573. https://doi.org/10.1007/s10029-022-02704-9 (2023).
19. Tuset, L. et al. Virtual simulation of the biomechanics of the abdominal wall with different stoma locations. *Sci. Rep.* **12**, 3545. https://doi.org/10.1038/s41598-022-07555-z (2022).
20. Tuset, L. et al. A virtual simulation approach to assess the effect of trocar-site placement and scar characteristics on the abdominal wall biomechanics. *Sci. Rep.* **14**, 3583. https://doi.org/10.1038/s41598-024-54119-4 (2024).
21. Rahbari, N. N. et al. Current practice of abdominal wall closure in elective surgery-is there any consensus?. *BMC Surg.* **9**, 1–8. https://doi.org/10.1186/1471-2482-9-8 (2009).
22. Singh, G. & Chanda, A. Mechanical properties of whole-body soft human tissues: A review. *Biomed. Mater.* **16**, 062004. https://doi.org/10.1088/1748-605X/ac2b7a (2021).
23. Rath, A. & Chevrel, J. The healing of laparotomies: Review of the literature. *Hernia* **2**, 145–149 (1998).
24. Laumonier, T. & Menetrey, J. Muscle injuries and strategies for improving their repair. *J. Exp. Orthop.* **3**, 15. https://doi.org/10.1186/s40634-016-0051-7 (2016).
25. Samartsev, V. A., Kuchumov, A. G. & Gavrilov, V. A. Sutures in abdominal surgery: Biomechanical study and clinical application. *Cent. Eur. J. Med.* **9**, 849–859. https://doi.org/10.2478/s11536-013-0334-7 (2014).
26. Hollinsky, C. & Sandberg, S. Measurement of the tensile strength of the ventral abdominal wall in comparison with scar tissue. *Clin. Biomech.* **22**, 88–92. https://doi.org/10.1016/j.clinbiomech.2006.06.002 (2007).
27. code Aster. Structures and thermomechanics analysis for studies and research (2020). https://www.code-aster.org/spip.php?rubrique2. Accessed 26-May-2020.
28. Fede, C. et al. Quantification of hyaluronan in human fasciae: Variations with function and anatomical site. *J. Anat.* **233**, 552–556. https://doi.org/10.1111/joa.12866 (2018).
29. Cobb, W. S. et al. Normal intraabdominal pressure in healthy adults. *J. Surg. Res.* **129**, 231–235. https://doi.org/10.1016/j.jss.2005.06.015 (2005).
30. Raghavan, M. L., Vorp, D. A., Federle, M. P., Makaroun, M. S. & Webster, M. W. Wall stress distribution on three-dimensionally reconstructed models of human abdominal aortic aneurysm. *J. Vasc. Surg.* **31**, 760–769. https://doi.org/10.1067/mva.2000.103971 (2000).
31. Blazek, D. et al. Systematic review of intra-abdominal and intrathoracic pressures initiated by the Valsalva Manoeuvre during high-intensity resistance exercises. *Biol. Sport* **36**, 373–386. https://doi.org/10.5114/biolsport.2019.88759 (2019).
32. Tuset, L., Fortuny, G., Herrero, J., Puigjaner, D. & López, J. M. Implementation of a new constitutive model for abdominal muscles. *Comput. Methods Programs Biomed.* **179**, 104988. https://doi.org/10.1016/j.cmpb.2019.104988 (2019).
33. Hernández-Gascón, B. et al. Understanding the passive mechanical behavior of the human abdominal wall. *Ann. Biomed. Eng.* **41**, 433–444. https://doi.org/10.1007/s10439-012-0672-7 (2013).
34. Lesch, C. et al. Standardized suturing can prevent slackening or bursting suture lines in midline abdominal incisions and defects. *Hernia* **26**, 1611–1623. https://doi.org/10.1007/s10029-022-02659-x (2022).
35. Cardoso, M. *Experimental Study of the Human Anterolateral Abdominal Wall: Biomechanical Properties of Fascia and Muscles*. Master's thesis, Universidade do Porto (2012). https://www.google.com/url?sa=t&source=web &rct=j &opi=89978449 &url=https://repositorio-aberto.up.pt/bitstream/10216/65576/1/000154315.pdf &ved=2ahUKEwj_jNTp0KyMAxWiVfEDHbMsFb0QFnoECB4QAQ &usg=AOvVaw1ml4qG0EPRlY5_UGUBvfFb. Accessed 28-March-2025.
36. Ben Abdelounis, H., Nicolle, S., Otténio, M., Beillas, P. & Mitton, D. Effect of two loading rates on the elasticity of the human anterior rectus sheath. *J. Mech. Behav. Biomed. Mater.* **20**, 1–5. https://doi.org/10.1016/j.jmbbm.2012.12.002 (2013).
37. Cooney, G. et al. Uniaxial and biaxial tensile stress–stretch response of human linea alba. *J. Mech. Behav. Biomed. Mater.* **63**, 134–140. https://doi.org/10.1016/j.jmbbm.2016.06.015 (2016).
38. Kriener, K. et al. Mechanical characterization of the human abdominal wall using uniaxial tensile testing. *Bioengineering* **10**, 1213. https://doi.org/10.3390/bioengineering10101213 (2023).
39. Miller, B. T. et al. Physiologic tension of the abdominal wall. *Surg. Endosc.* **37**, 9347–9350. https://doi.org/10.1007/s00464-023-10346-w (2023).
40. Baygutalp, F., Razmi, A. & Mustafaoglu, M. Finite element analysis of lumbosacral soft tissue at sitting posture at desktop computer. *Ann. Med. Res.* **30**, 7–13. https://doi.org/10.5455/annalsmedres.2022.03.109 (2023).
41. Yousefi, A. A. K., Pierrat, B., Ruyet, A. L. & Abril, S. Patient-specific computational simulations of wound healing following midline laparotomy closure. *Biomech. Model. Mechanobiol.* **22**, 1589–1605. https://doi.org/10.1007/s10237-023-01708-3 (2023).
42. Deerenberg, E. B. et al. Updated guideline for closure of abdominal wall incisions from the European and American hernia societies. *Br. J. Surg.* **109**, 1239–1250 (2022).
43. Williams, T., Kelley, C., Lang, R., Kotz, D., Campbell, J., Elber, G., Woo, A. et al.. Gnuplot 6.0: an interactive plotting program. https://gnuplot.sourceforge.net/ (2025). Accessed 14-Apr-2025.
44. kitware. Paraview. https://www.paraview.org (2025). Accessed 14-Apr-2025.

Acknowledgements

This project has been partially founded by AGAUR research group 2021SGR-00111: "ASCLEPIUS: Smart Technology for Smart Healthcare". All the images included in the figures have been created by the authors. All two-dimensional images ($x - y$ plots) have been generated using the open source gnuplot 5.4 software (https://gnuplo

t.sourceforge.net/)[43]. All three-dimensional images (Figs. 1a–f, 2a–e, 3a–f, 4f, 5a–i, 6d, 7a–d, 8a–h, 9a–f and 10f) have been generated using the open source ParaView 5.9 software (https://www.paraview.org)[44].

Author contributions

Conception: M.L.-C. and G.F. Simulation design and setup: L.T., G.F., J.M.L., J.H. and D.P. Performing the simulations: L.T. Post-processing: L.T., G.F., J.M.L., J.H. and D.P. All authors analyzed and discussed the results of the simulations. All authors contributed to the writing of the manuscript. All authors have read and agreed to the submitted version of the manuscript.

Declarations

Competing interests

The authors declare no competing interests.

Additional information

Correspondence and requests for materials should be addressed to D.P.

Reprints and permissions information is available at www.nature.com/reprints.

Publisher's note Springer Nature remains neutral with regard to jurisdictional claims in published maps and institutional affiliations.